

## High-pressure Raman scattering in wurtzite indium nitride

J. Ibáñez,<sup>1,a)</sup> F. J. Manjón,<sup>2</sup> A. Segura,<sup>3</sup> R. Oliva,<sup>1</sup> R. Cuscó,<sup>1</sup> R. Vilaplana,<sup>4</sup> T. Yamaguchi,<sup>5</sup> Y. Nanishi,<sup>5</sup> and L. Artús<sup>1</sup>

<sup>1</sup>Institut Jaume Almera, Consell Superior d'Investigacions Científiques, 08028 Barcelona, Catalonia, Spain

<sup>2</sup>Instituto de Diseño para la Fabricación y Producción Automatizada, MALTA Consolider Team-Universitat Politècnica de València, 46022 València, Spain

<sup>3</sup>Departamento de Física Aplicada-ICMUV-MALTA Consolider Team, Universitat de València, 46100 Burjassot, València, Spain

<sup>4</sup>Centro de Tecnologías Físicas, MALTA Consolider Team-Universitat Politècnica de València, 46022 València, Spain

<sup>5</sup>Faculty of Science and Engineering, Ritsumeikan University, Shiga 525-8577, Japan

(Received 2 May 2011; accepted 20 June 2011; published online 7 July 2011)

We perform Raman-scattering measurements at high hydrostatic pressures on *c*-face and *a*-face InN layers to investigate the high-pressure behavior of the zone-center optical phonons of wurtzite InN. Linear pressure coefficients and mode Grüneisen parameters are obtained, and the experimental results are compared with theoretical values obtained from *ab initio* lattice-dynamical calculations. Good agreement is found between the experimental and calculated results. © 2011 American Institute of Physics. [doi:10.1063/1.3609327]

Over the last few years, indium nitride (InN) has received intensive research interest because of its great potential to develop a wide variety of applications such as high-frequency electronic devices, high-efficiency tandem solar cells, or infrared light-emitting devices.<sup>1</sup> Although the growth of high quality InN is still challenging, bulk material with residual electron densities lower than  $5 \times 10^{17} \text{ cm}^{-3}$  and electron mobilities higher than  $2000 \text{ cm}^2 \text{ V}^{-1} \text{ s}^{-1}$  has been achieved by molecular beam epitaxy (MBE).<sup>2</sup> In spite of the great interest of InN from both fundamental and applied points of view, many material properties of this compound remain to be investigated. The production of high-quality InN layers and the discovery of the 0.7 eV fundamental band gap of wurtzite InN (w-InN) made necessary to revise many material parameters of InN and InN-based alloys, including their high-pressure behavior.<sup>3,4</sup>

While the available experimental data on the vibrational properties of InN stem mainly from Raman spectroscopy (see for instance Ref. 5 and references therein), a deeper understanding of the lattice dynamics in InN has only been accomplished very recently by means of grazing incidence inelastic x-ray scattering (IXS) measurements on high-quality InN epilayers.<sup>6</sup> Regarding the high-pressure vibrational properties of InN, Piquier *et al.*<sup>7,8</sup> used Raman scattering to study the pressure dependence of the  $E_{2h}$ ,  $A_1$  (TO), and  $A_1$  (LO) phonon modes of w-InN in a layer with a high background electron concentration ( $2.3 \times 10^{19} \text{ cm}^{-3}$ ). These authors observed the wurtzite-to-rocksalt transition and studied the pressure dependence, up to 50 GPa, of broad bands arising from the rocksalt phase.<sup>8</sup> However, the pressure dependence of the long-lived  $E_{2l}$  mode and of the  $E_1$  modes of w-InN was not reported in those works. Recently, Yao and co-workers employed Raman scattering to investigate the structural stability of poorly crystalline w-InN nanowires under high pressure.<sup>9</sup> The pressure coefficients and mode Grüneisen parameters obtained by these authors for the  $A_1$

(TO),  $E_{2h}$ , and  $A_1$  (LO) modes were sizably lower than those reported in Refs. 7 and 8.

In this letter, we present Raman-scattering measurements under high hydrostatic pressure on high-quality *c*-face and *a*-face InN epilayers grown by MBE. Experiments on both types of samples have allowed us to study the pressure behavior of the non-polar  $E_{2l}$  and  $E_{2h}$  optical phonons and of the polar  $A_1$  (TO),  $E_1$  (TO), and LO phonons of w-InN. The linear pressure coefficients and mode Grüneisen parameters of these modes have been determined and found to be in good agreement with the results of *ab initio* lattice-dynamical calculations based on density functional theory (DFT).

For the present study, we used two different w-InN epilayers, with thicknesses of  $5.7 \mu\text{m}$  (*c*-face) and 500 nm (*a*-face). Both samples were grown by plasma assisted MBE on sapphire substrates. The background electron concentration of the samples was  $\sim 1 \times 10^{18} \text{ cm}^{-3}$  (*c*-face) and  $\sim 4 \times 10^{18} \text{ cm}^{-3}$  (*a*-face). Flakes of w-InN containing some residual sapphire were detached from the substrate and loaded in a gasketed membrane-type diamond anvil cell (DAC) with  $400 \mu\text{m}$  culet-size diamonds. Methanol-ethanol-water (16:3:1) was employed as pressure transmitting medium, and the ruby fluorescence method was used to determine the applied pressure. Confocal micro-Raman measurements at room temperature were acquired with a HORIBA Jobin-Yvon LabRam-HR spectrometer. To reduce the Rayleigh radiation and to detect the low-frequency  $E_{2l}$  mode of w-InN by means of a single-grating spectrometer such as the LabRam-HR system, we used the 632.8-nm line of a He-Ne laser as excitation radiation. A  $50\times$  objective was employed to focus the laser beam and to collect the scattered radiation. In the case of the *c*-face sample, the measurements were carried out up to the transition pressure, which was observed to begin at  $\sim 12$  GPa in this sample. For the *a*-face sample, the experiments were performed up to a pressure of  $\sim 10$  GPa.

Figures 1 and 2 show selected Raman spectra at different pressures for the *c*-face and the *a*-face epilayers, respectively. As expected from the selection rules for Raman experiments in backscattering geometry on a *c* face of

<sup>a)</sup> Author to whom correspondence should be addressed. Electronic mail: jibanez@ictja.csic.es.

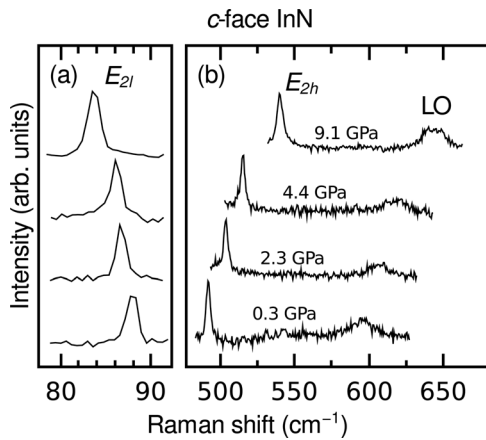


FIG. 1. Room-temperature Raman spectra of a *c*-face InN layer at different hydrostatic pressures in the up-stroke (a) in the low-frequency region and (b) in the high-frequency region.

wurtzite crystals, the spectra of Fig. 1 are dominated by the non-polar  $E_{2l}$  and  $E_{2h}$  modes of w-InN [Figs. 1(a) and 1(b), respectively]. The weak band that appears in the high-frequency region of the spectra in Fig. 1(b) contains contributions of both  $A_1$  (LO) and  $E_1$  (LO) modes. Note that, at ambient pressure, the Raman spectra of as-grown *c*-face epilayers display the expected  $A_1$  (LO) mode and also some weaker signal arising from the forbidden  $E_1$  (LO) mode. The observation of  $E_1$  (LO) signal through impurity-induced Fröhlich interaction in the spectra of *c*-face InN layers is attributed to the relaxation of the selection rules induced by defects.<sup>10</sup> When the InN material is loaded into the DAC, the LO band is found to broaden and shift to higher frequencies, while the dominant  $E_{2h}$  peak remains basically unchanged. This suggests that sample misorientation and/or disorder generated during the sample loading give rise to a further enhancement of the  $E_1$  (LO) signal. Similarly, in the case of the *a*-face epilayer both the  $A_1$  (LO) and  $E_1$  (LO) modes are symmetry forbidden and they become visible through impurity scattering [Fig. 2(b)]. The spectra of the *a*-face sample also exhibit the  $A_1$  (TO) and  $E_1$  (TO) modes, which show up as weak features below the  $E_{2h}$  peak [Fig. 2(a)]. Among all the modes observed in this work, the low-intensity TO peaks

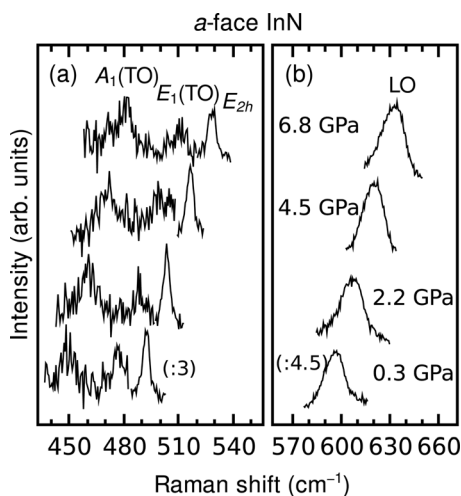


FIG. 2. Room-temperature Raman spectra of an *a*-face InN layer at different hydrostatic pressures in the up-stroke (a) in the middle-frequency region and (b) in the high-frequency region.

yield the highest error in the frequency measurement, which we estimate is lower than  $2 \text{ cm}^{-1}$ . The  $E_{2l}$  peaks detected in the case of the *a*-face epilayer (not shown) were fairly weak, superimposed to a relatively strong background signal.

Both Figs. 1 and 2 show the expected frequency increase for all phonon modes with increasing pressure, with the exception of the  $E_{2l}$  mode, which displays a pressure-induced softening. This behavior is typical of shear phonon modes, i.e., zone-edge transverse acoustic (TA) modes in zincblende and diamond semiconductors.<sup>11</sup> In general, it is found that the mode Grüneisen parameter of the soft mode linearly correlates to the transition pressure of the material.<sup>12,13</sup> In the case of wurtzite compounds, the  $E_{2l}$  mode corresponds to the TA(L) mode of the zincblende structure due to the folding of the zone-edge TA modes along the  $\Gamma$ -L direction of the Brillouin zone. The softening of the  $E_{2l}$  mode has been observed in many different wurtzite compounds, including ZnO (Ref. 14) and GaN (Ref. 15). Only AlN (Refs. 13 and 16) and BeO (Ref. 17) seem not to exhibit this softening behavior. While the positive pressure coefficient for the  $E_{2l}$  mode of BeO is probably linked with its high pressure stability, the case of AlN is somewhat puzzling, since the wurtzite-to-rocksalt transition occurs at a relatively low pressure ( $\sim 20$  GPa). The observation of positive pressure coefficients for the  $E_{2l}$  mode of AlN might be related to the special balance between ionic and covalent restoring forces in this compound.<sup>11</sup> In the case of InN, following the discussion of Ref. 12, the observed softening of the  $E_{2l}$  mode is consistent with the observed transition pressures, around 12–14 GPa.<sup>8,18</sup>

In Fig. 3, we have plotted the pressure dependence of the measured optical phonon frequencies. Data obtained for the two samples studied in this work have been included in the figure. Note the similar pressure behavior observed for the  $E_{2h}$  and LO modes in both samples. Table I displays the linear pressure coefficients ( $a_i$ ) extracted with a linear fit to all the experimental data, i.e., employing the expression  $\omega_i(P) = \omega_i(0) + a_i P$ , where  $\omega_i(P)$  is the frequency of the  $i$ th mode at a pressure  $P$ . Mode Grüneisen parameters for the  $i$ th mode,  $\gamma_i$ , are subsequently deduced by using the expression  $\gamma_i = B_0 a_i / \omega_i(0)$ , where  $B_0$  is the bulk modulus of the material. Here, we use a value of  $B_0 = 143$  GPa, which we obtain from DFT *ab initio* calculations (see details in Ref. 5). This value

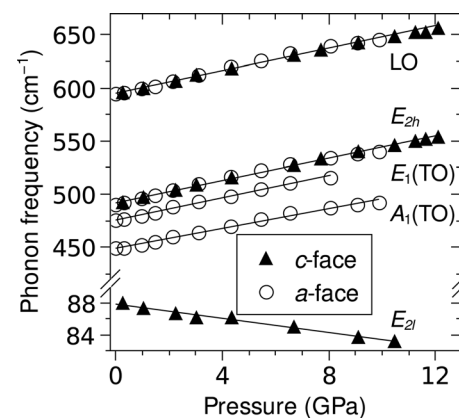


FIG. 3. Pressure dependence of the optical phonon frequencies of w-InN measured in the up-stroke in *c*-face InN (solid triangles) and *a*-face InN (open circles). The lines are the results of linear fits to the experimental data.

TABLE I. Results of the linear fits to the pressure behavior of the optical phonons of w-InN.  $\omega_i(0)$  and  $a_i$  are the zero-pressure frequency and the linear pressure coefficient for the  $i$ th mode, respectively. A bulk modulus of 143 GPa was used to obtain the mode Grüneisen parameters ( $\gamma_i$ ). Values in parentheses are the results of *ab initio* lattice-dynamical calculations. Theoretical values for the LO mode correspond to the  $A_1$  (LO) phonon.

Phonon mode $i$	$\omega_i(0)$ (cm <sup>-1</sup> )	$a_i$ (cm <sup>-1</sup> GPa <sup>-1</sup> )	$\gamma_i$
$E_{2l}$	88 (83.9)	-0.4 (-0.63)	-0.65 (-1.07)
$A_1$ (TO)	449 (450.4)	5.3 (4.69)	1.69 (1.49)
$E_1$ (TO)	476 (474.5)	5.3 (4.88)	1.59 (1.47)
$E_{2h}$	492 (488.4)	5.2 (5.18)	1.51 (1.52)
LO	595 (591.8)	5.1 (4.87)	1.22 (1.17)

is in close agreement to that obtained recently with grazing incidence IXS measurements ( $B_0 = 152$  GPa).<sup>6</sup> We plot in Fig. 3 the results of linear fits to the experimental data (solid lines). The resulting mode Grüneisen parameters for the different phonons are displayed in the last column of Table I.

The  $a_i$  values obtained with our high-pressure Raman experiments for the TO,  $E_{2h}$ , and LO modes of InN are lower than those reported in InN films with much higher residual electron densities.<sup>7,8</sup> In contrast, the  $a_i$  values obtained by Yao *et al.*<sup>9</sup> on InN nanowires are even lower than those measured here. Given that several possible sources of unintentional doping have been reported in InN, the origin of the different pressure behavior observed in samples with different electron densities cannot be established. More work would be necessary in order to clarify this issue.

From the experimental data obtained with the present measurements (Table I), it can be seen that the pressure behavior of the  $A_1$  (TO) phonons of w-InN (ionic vibrations along the  $c$ -axis) is similar to that of the  $E_{2h}$  and  $E_1$  (TO) modes (vibrations perpendicular to the  $c$ -axis). GaN exhibits a similar behavior.<sup>19</sup> This is in contrast, for instance, to the case of w-AlN, where the measured pressure coefficients for the  $E_1$  and  $E_{2h}$  modes are much larger than for the  $A_1$  modes.<sup>16</sup>

To gain further insight into the pressure behavior of the phonons of w-InN, we have performed *ab initio* lattice-dynamical calculations of the linear pressure coefficients ( $a_i$ ) and mode Grüneisen parameters ( $\gamma_i$ ) for the zone-center optical phonons of this compound. The calculations, based on DFT within the local density approximation (LDA), were carried out with the ABINIT package.<sup>20</sup> Calculations were performed at different pressures, and  $a_i$  and  $\gamma_i$  values were obtained with a linear fit to the data. Details of the calculations at ambient pressure can be found elsewhere.<sup>5</sup> Since the ABINIT code fails to correctly predict the dispersion of the  $E_1$  (LO) mode in wurtzite materials,<sup>5</sup> the calculated values for the LO phonon given in Table I correspond to the  $A_1$  (LO) phonon. The resulting  $a_i$  and  $\gamma_i$  values are displayed in parentheses in Table I. Good agreement is found between the experimental data obtained in the present work and the calculated values for the TO and the non-polar modes. In contrast, the theoretical  $a_i$  values are systematically lower than those previously measured in bulk w-InN.<sup>7,8</sup> Remarkably, the DFT-LDA calculations predict the softening of the  $E_{2l}$  mode, as observed with the present measurements. Note also that the DFT calculations predict a very small increase of the  $A_1$  (LO)- $A_1$  (TO) splitting ( $\sim 0.18$  cm<sup>-1</sup> GPa<sup>-1</sup>). Instead,

we observe a small decrease of  $\sim -0.2$  cm<sup>-1</sup> GPa<sup>-1</sup> for the LO band in relation to both the  $A_1$  (TO) and the  $E_1$  (TO) modes. Within the experimental error of the present measurements, this result confirms that only a very small pressure dependence of the LO-TO splitting may be expected in w-InN. Finally, we would like to remark that, leaving aside the soft  $E_{2l}$  mode, the *ab initio* calculations predict a very similar pressure behavior for all the Raman-active modes of w-InN regardless of the direction of the ionic vibrations, which is in agreement with the experimental results.

In conclusion, we have performed high-pressure Raman measurements on  $c$ -face and  $a$ -face layers to investigate the pressure behavior of the zone-center optical phonons of wurtzite InN. The linear pressure coefficient and mode Grüneisen parameters of the  $E_{2l}$ ,  $A_1$  (TO),  $E_1$  (TO),  $E_{2h}$ , and LO modes of w-InN have been obtained. Good agreement between the experimental data and theoretical values obtained with *ab initio* lattice-dynamical calculations has been found.

Work supported by the Spanish MICINN (Projects MAT2010-16116, MAT2008-06873-C02-02, MAT2010-21270-C04-04, and CSD2007-00045), the Catalan Government (BE-DG 2009), and the Spanish Council for Research (PIE2009-CSIC).

<sup>1</sup>*Indium Nitride and Related Alloys*, edited by T. D. Veal, C. F. McConville, and W. J. Schaff (CRC/Taylor and Francis, Boca Raton, 2009).

<sup>2</sup>C. S. Gallinat, G. Koblmüller, J. S. Brown, S. Bernardis, J. S. Speck, G. D. Chern, E. D. Readinger, H. Shen, and M. Wraback, *Appl. Phys. Lett.* **89**, 032109 (2006).

<sup>3</sup>S. X. Li, J. Wu, E. E. Haller, W. Walukiewicz, W. Shan, H. Lu, and W. J. Schaff, *Appl. Phys. Lett.* **83**, 4963 (2003).

<sup>4</sup>I. Gorczyca, J. Plesiewicz, L. Dmowski, T. Suski, N. E. Chistensen, A. Svane, C. S. Gallinat, G. Koblmüller, and J. S. Speck, *J. Appl. Phys.* **104**, 013704 (2008).

<sup>5</sup>N. Domènech-Amador, R. Cuscó, L. Artús, T. Yamaguchi, and Y. Nanishi, *Phys. Rev. B* **83**, 245203 (2011).

<sup>6</sup>J. Serrano, A. Bosak, M. Krisch, F. J. Manjón, A. H. Romero, N. Garro, X. Wang, A. Yoshikawa, and M. Kuball, *Phys. Rev. Lett.* **106**, 205501 (2011).

<sup>7</sup>C. Piquier, F. Demangeot, J. Frandon, J. W. Pomeroy, M. Kuball, H. Hubel, N. W. A. van Uden, D. J. Dunstan, O. Briot, B. Maleyre, S. Ruffenach, and B. Gil, *Phys. Rev. B* **70**, 113202 (2004).

<sup>8</sup>C. Piquier, F. Demangeot, J. Frandon, J. C. Chervin, A. Polian, B. Couzinet, P. Munsch, O. Briot, S. Ruffenach, B. Gil, and B. Maleyre, *Phys. Rev. B* **73**, 115211 (2006).

<sup>9</sup>L. D. Yao, S. D. Luo, X. Shen, S. J. You, L. X. Yang, S. J. Zhang, S. Jiang, Y. C. Li, J. Liu, K. Zhu, Y. L. Liu, W. Y. Zhou, L. C. Chen, C. Q. Jin, R. C. Yu, and S. S. Xie, *J. Mater. Res.* **25**, 2330 (2010).

<sup>10</sup>R. Cuscó, J. Ibáñez, E. Alarcón-Lladó, L. Artús, T. Yamaguchi, and Y. Nanishi, *Phys. Rev. B* **79**, 155210 (2009).

<sup>11</sup>J. M. Wagner and F. Bechstedt, *Phys. Status Solidi B* **235**, 464 (2003).

<sup>12</sup>B. A. Weinstein, *Solid State Commun.* **24**, 595 (1977).

<sup>13</sup>E. V. Yakovenko, M. Gauthier, and A. Polian, *JETP* **98**, 981 (2004).

<sup>14</sup>J. S. Reparaz, L. R. Muniz, M. R. Wagner, A. R. Goñi, M. I. Alonso, A. Hoffmann, and B. K. Meyer, *Appl. Phys. Lett.* **96**, 231906 (2010).

<sup>15</sup>P. Perlin, C. Jaubertie-Carillon, J. P. Itié, A. San Miguel, I. Grzegory, and A. Polian, *Phys. Rev. B* **45**, 83 (1992).

<sup>16</sup>F. J. Manjón, D. Errandonea, A. H. Romero, N. Garro, J. Serrano, and M. Kuball, *Phys. Rev. B* **77**, 205204 (2008).

<sup>17</sup>A. P. Jephcoat, R. J. Hemley, H. K. Mao, R. E. Cohen, and M. J. Mehl, *Phys. Rev. B* **37**, 4727 (1988).

<sup>18</sup>J. Ibáñez, A. Segura, F. J. Manjón, L. Artús, T. Yamaguchi, and Y. Nanishi, *Appl. Phys. Lett.* **96**, 201903 (2010).

<sup>19</sup>A. R. Goñi, H. Siegle, K. Syassen, C. Thomsen, and J.-M. Wagner, *Phys. Rev. B* **64**, 035205 (2001).

<sup>20</sup>The ABINIT code is a common project of the Université Catholique de Louvain, Corning Incorporated, and other contributors (<http://www.abinit.org>).